Glia

WILEY
GLIA

RESEARCH ARTICLE

Trifluoperazine Elevates Intracellular Ca^{2+} Levels and Locks Open the Store-Operated Calcium Entry Channels in Astrocytes

Jiwoon Lim[1,2] | Wongu Youn[1] | C. Justin Lee[1,2]

[1]Cognitive Glioscience Group, Center for Cognition and Sociality, Institute for Basic Science (IBS), Daejeon, Republic of Korea | [2]IBS School, University of Science and Technology (UST), Daejeon, Republic of Korea

Correspondence: C. Justin Lee (cjl@ibs.re.kr)

Received: 12 February 2025 | **Revised:** 30 May 2025 | **Accepted:** 5 June 2025

Funding: This study was supported by the Center for Cognition and Sociality (IBS-R001-D2) to C.J.L. from the Institute for Basic Science (IBS), South Korea.

Keywords: astrocyte | calmodulin | STIM1–Orai complex | store-operated calcium entry | trifluoperazine

ABSTRACT

Trifluoperazine (TFP), a known inhibitor of Ca^{2+}-bound calmodulin (Ca^{2+}/CaM), has been reported to elevate cytosolic Ca^{2+} levels by disinhibiting inositol 1,4,5-triphosphate receptor 2 (IP_3R2), thereby suppressing glioblastoma invasion and inducing apoptosis. Interestingly, TFP induces a sustained Ca^{2+} plateau, sensitive to extracellular Ca^{2+}, suggesting involvement of Ca^{2+} entry such as store-operated calcium entry (SOCE). However, the underlying molecular mechanism remains elusive. Here, we report that TFP induces sustained Ca^{2+} signals by blocking the Ca^{2+}/CaM-dependent desensitization of SOCE channels in cortical astrocyte cultures. TFP induces a prolonged Ca^{2+} response, with distinct kinetics compared to other Ca^{2+} modulators such as TFLLR-NH_2 (a $G_{\alpha q}$-coupled GPCR agonist) and thapsigargin (a sacro/endoplasmic reticulum Ca^{2+}-ATPase inhibitor). Under extracellular Ca^{2+}-free conditions, Ca^{2+} levels increase without reaching a plateau, suggesting that the sustained Ca^{2+} signal relies on Ca^{2+} influx. Pharmacological analysis shows that sustained Ca^{2+} signals by TFP are CaM-dependent. Gene silencing targeting STIM1 and Orai1–3 confirmed their essential roles in the sustained response. We find that TFP effectively "locks open" SOCE channels by inhibiting their desensitization, maintaining SOCE activity. This effect is also observed in ex vivo hippocampal dentate gyrus astrocytes. Structural modeling supports a mechanism in which TFP disrupts the interaction between Ca^{2+}/CaM and the SOAR domain of STIM1. Together, these findings indicate that TFP elevates cytosolic Ca^{2+} levels by maintaining SOCE activation, offering novel insights into the molecular actions of this drug. TFP can be a pharmacological tool for SOCE research as it locks SOCE channels open.

1 | Introduction

Ca^{2+} serves as a key signaling molecule in organisms, regulating a variety of biological processes such as proliferation, exocytosis, and cell death (Giorgi et al. 2018). While cytosolic Ca^{2+} levels are kept low, Ca^{2+} is stored in organelles such as the endoplasmic reticulum (ER) and lysosomes (Rizzuto and Pozzan 2006). Diverse stimuli activate the phospholipase C family, generating inositol-1,4,5-triphosphate (IP3) and inducing Ca^{2+} release from the ER via the opening of the inositol 1,4,5-triphosphate receptor (IP3R) (Clapham 2007). After Ca^{2+} release from the ER, cells rely on specific mechanisms to restore depleted Ca^{2+} levels. One of the strategies for Ca^{2+} homeostasis in the cell is store-operated calcium entry (SOCE) (Putney Jr 1986). Following the activation of G-protein-coupled receptors, ER Ca^{2+} stores are depleted, triggering the stromal interaction molecule (STIM) in

the ER membrane via sensing low Ca^{2+} levels (Liou et al. 2005; Roos et al. 2005). STIM then interacts with calcium release-activated calcium channel protein (Orai) channels in the plasma membrane, mediating Ca^{2+} influx from the extracellular environment to replenish ER Ca^{2+} stores (Feske et al. 2006; Vig et al. 2006; Zhang et al. 2006). With SOCE, cytosolic Ca^{2+} levels are increased, and Ca^{2+}-dependent inhibition (CDI) of SOCE is turned on (Fierro and Parekh 1999; Hoth and Penner 1993; Li et al. 2017; Maléth et al. 2014; Zweifach and Lewis 1995). Various pharmacological tools have been developed to modulate SOCE. However, most available drugs function as SOCE inhibitors, and no pharmacological agent has been identified to prolong the open state of SOCE (Prakriya and Lewis 2015).

One mechanism underlying CDI is calmodulin (CaM)-dependent regulation (Li et al. 2017). CaM, a highly conserved Ca^{2+} binding protein, is an essential protein for Ca^{2+}-dependent signaling (Clapham 2007). Ca^{2+} unbound CaM (Apo-calmodulin) becomes an elongated structure by Ca^{2+} binding, and Ca^{2+}/CaM binds to proteins, affecting Ca^{2+}-dependent signaling in the organism (Meador et al. 1992). Several CaM inhibitors have been developed and identified to investigate the role of CaM. Trifluoperazine (TFP), initially developed as a treatment for schizophrenia and anxiety, has been utilized as a CaM inhibitor (Weiss et al. 1982). TFP binds to Ca^{2+}/CaM and changes the secondary structure of Ca^{2+}/CaM, blocking interaction between Ca^{2+}/CaM and target proteins (Vandonselaar et al. 1994).

Recently, TFP has garnered attention for its anticancer properties, including the induction of apoptosis, inhibition of proliferation and metastasis, and modulation of drug resistance in cancer cells (Feng et al. 2018; Xia et al. 2019; Yeh et al. 2012). Our prior research demonstrated that TFP inhibits tumor growth and glioblastoma invasion by inducing elevation of cytosolic Ca^{2+} levels via disinhibition of IP3R. Notably, TFP-induced Ca^{2+} elevation is characterized by sustained kinetics, with no decay over time. Prolonged cytosolic Ca^{2+} elevation, which is the cause of apoptosis of glioblastoma cells, seems to originate from extracellular Ca^{2+} (Kang et al. 2017). Cells have diverse strategies for Ca^{2+} uptake from extracellular space. SOCE is the major source of the influx of extracellular Ca^{2+} in the cells, suggesting the possibility that SOCE is involved in the TFP-induced Ca^{2+} elevation. However, the molecular mechanism underlying this sustained cytosolic Ca^{2+} elevation remains unclear.

In this study, we investigated the veiled mechanism of sustained TFP-induced Ca^{2+} elevation using primary astrocyte cultures. Our findings revealed biphasic concentration dependence and unique kinetics of TFP-induced Ca^{2+} signals. Extracellular Ca^{2+} and CaM were shown to play key roles in maintaining these signals. Gene silencing of Stim1 and Orai1/2/3 revealed the involvement of the SOCE system in sustaining TFP-induced Ca^{2+} signals. Using a SOCE induction protocol for Ca^{2+} imaging, we found that TFP locks SOCE open by inhibiting desensitization. Also, we verified that astrocytes in brain slices also show similar sustained Ca^{2+} elevation by TFP treatment. Furthermore, we confirmed that TFP reduces binding stability between Ca^{2+}/CaM and the SOAR domain of STIM1 via protein–protein docking modeling. Thus, we propose that TFP sustains Ca^{2+} signals by maintaining the SOCE system in an open state and provides novel insight into how TFP can cause Ca^{2+}-dependent apoptosis.

2 | Materials and Methods

2.1 | Primary Cell Culture

Primary cortical astrocytes were prepared from 1-day postnatal C57BL/6 mice as previously described (Woo et al. 2012). The cerebral cortex was dissected free of adherent meninges, minced, and dissociated into a single-cell suspension by trituration. Dissociated cells were plated onto plates coated with 0.1 mg/mL poly-D-lysine (Sigma). Cells were grown in Dulbecco's modified Eagle's medium (DMEM, Corning) supplemented with 4.5 g/L glucose, L-glutamine, sodium pyruvate, 10% heat-inactivated horse serum, 10% heat-inactivated fetal bovine serum, and 1000 units/mL of penicillin–streptomycin. Cultures were maintained at 37°C in a humidified atmosphere containing 5% CO_2. Three days later, cells were vigorously washed with repeated pipetting using medium, and the media were replaced to remove debris and other floating cell types.

2.2 | Animals

All C57BL/6 mice were group-housed in a temperature- and humidity-controlled environment with a 12 h light/dark cycle and had free access to food and water. All animal care and handling were approved by the Institutional Animal Care and Use Committee of the Institute for Basic Science (IBS-2025-013; Daejeon, Korea). For the slice patch, 8- to 20-week-old male C57BL/6 mice were used.

2.3 | Chemicals

During Ca^{2+} imaging, trifluoperazine dihydrochloride (Sigma), proteinase-activated receptor 1 (PAR1) agonist; TFLLR-NH_2 (Peptron), sarco/endoplasmic reticulum Ca^{2+}-ATPase (SERCA) inhibition; thapsigargin (Tocris), ethylene glycol-bis-*N*,*N*,*N*′,*N*′-tetraacetic acid (Sigma) and calmodulin inhibitor; W-7 hydrochloride (Tocris) were used.

2.4 | shRNA Sequences

The targeted genes (known RefSeq from Pubmed) for shRNA development are mOrai1 (NM_175423.3), mOrai2 (NM_178751.3), mOrai3 (NM_198424.3), and mStim1 (NM_009287.4). Target sequences are as follows:

Stim1, 5′-GCGAGATGAGATCAACCTTGC-3′; Oria1, 5′-GCACCTGTTTGCCCTCATGAT-3′; Orai2, 5′-GCCACAAGGGCATGGATTACC-3′; Orai3, 5′-GGGTCAAGTTTGTGCCCATTG-3′.

2.5 | Ca^{2+} Imaging (In Vitro)

For imaging, cultured astrocytes were plated as a monolayer (5×10^3 cells/mL) on 12-mm glass coverslips coated with poly-D-lysine at DIV 10, and Ca^{2+} imaging was conducted at DIV 13-14 at room temperature. On the imaging day, astrocytes were incubated with 5 μM Fura-2AM and 1 μM pluronic acid (Thermo Fisher) for 30 min at room temperature. The external

solution contained 150 mM NaCl, 10 mM HEPES, 3 mM KCl, 2 mM $CaCl_2$, 1 mM $MgCl_2$, 22 mM sucrose, and 10 mM glucose (pH adjusted to 7.4 and osmolarity to 325 mOsm), and for the Ca^{2+}-free external solution, 200 nm EGTA (Sigma) was substituted for $CaCl_2$. Imaging Workbench version 9.0 (Bluecell) was used for the acquisition of intensity images and conversion to ratios, as previously described (Kang et al. 2010). For gene silencing, at DIV10, the shRNA plasmid vector was transfected into cultured astrocytes using the Neon transfection system (Thermo Fisher), and Ca^{2+} imaging was conducted at DIV14. For live imaging, cells were visualized using a 20× Nikon objective (NIR S Fluor, 20/0.75, DIC M/N2, ∞/0.17 WD 1.0) equipped with infrared differential interference contrast (IR-DIC) optics. pE-340fura (CoolLED) was used for the light source, and light illumination was obtained using 340 and 380 nm excitation. Images were taken at a frequency of 1 Hz, and the exposure time of light illumination was 0.05 s for both wavelengths.

Baseline signals were recorded for 60 s, and drugs were applied through a bath application system. The detailed timing of drug treatments is labeled in the figures. For analyzing the desensitization of SOCE with imaging techniques, we adopted a protocol from previous reports (Kwon et al. 2017). Cultured astrocytes were incubated in Ca^{2+}-free solution. After obtaining the baseline, cultured astrocytes were treated with thapsigargin, a SERCA inhibitor, to deplete Ca^{2+} in the ER. After stabilization of the baseline, 2 mM Ca^{2+} was introduced to the cultured astrocytes. We analyzed the desensitization index by dividing the delta value of the Fura-2 ratio at 390 s after 2 mM Ca^{2+} administration (decay amplitude) by the delta value of the Fura-2 ratio at 135 s after 2 mM Ca^{2+} administration (peak amplitude). TFP was applied 100 s before 2 mM Ca^{2+} administration.

2.6 | Ca^{2+} Imaging (Ex Vivo)

Mice were anesthetized with isoflurane and decapitated to remove the brain. The brains were sectioned in ice-cold slicing solution containing 212.5 mM sucrose, 3 mM KCl, 1.25 mM NaH_2PO_4, 26 mM $NaHCO_3$, 5 mM $MgCl_2$, 0.1 mM $CaCl_2$, and 10 mM glucose. Horizontal slices (300 μm thick) were prepared with a vibrating-knife microtome Linear Slicer Pro7 (D.S.K). For stabilization, slices were incubated at room temperature for at least 1 h in a solution containing 130 mM NaCl, 3.5 mM KCl, 1.25 mM NaH_2PO_4, 24 mM $NaHCO_3$, 1.5 mM $MgCl_2$, 1.5 mM $CaCl_2$-$2H_2O$, and 10 mM glucose and simultaneously equilibrated with 95% O_2/5% CO_2 at 25°C.

Prepared slices were transferred to a recording chamber that was continuously perfused with ACSF solution (flow rate, 2 mL min^{-1}). The slice chamber was mounted on the stage of an upright Zeiss microscope and viewed with a 63× water immersion objective (0.90 numerical aperture) with infrared differential interference contrast optics. Cellular morphology was visualized by a charge-coupled device camera (Hamamatsu) and Imaging Workbench software. Whole-cell patch was made from astrocyte somata located in the DG. The holding potential was −80 mV. Pipettes (resistance 8–10 MΩ) were filled with internal solution containing 60 mM KCl, 80 mM K-gluconate, 10 mM HEPES, 1 mM Calcium Green-1 dextran (Invitrogen), pH 7.35 with an osmolarity, 278–285 mOsmol/kg. Astrocytes were identified by their characteristic morphology, passive conductance, and negative resting membrane potential. For assessing passive conductance, a voltage step protocol was applied ranging from −180 to 20 mV in 20 mV intervals. The rectification index was calculated as the difference in current between +20 and −80 mV, divided by the difference in current between −80 and −180 mV. After a stable dialysis period of 10 min, Ca^{2+} imaging was conducted. pE-340fura (CoolLED) was used for light source, and light illumination was obtained using 488 nm excitation. Images were taken in 1 Hz frequency and exposure time of light illumination was 0.01 s. Baseline signals were recorded for 4 min, and drugs were applied through a bath application system. The detailed timing of drug treatments is labeled in the figures.

2.7 | In Silico Modeling for Protein–Protein Docking

For in silico modeling for protein–protein docking, the structures of proteins (1EXR for Ca^{2+}/CaM, 1LIN TFP-bound Ca^{2+}/CaM, and 3TEQ for SOAR domain of STIM1) were adopted from PDB and prepared using protein preparation workflow tool of Maestro (version 14.2, Schrodinger LLC) (Vandonselaar et al. 1994; Wilson and Brunger 2000; Yang et al. 2012). Protein structures were built and prepared in the environment of pH 7.40 ± 1.0 using Epic ionizer and energetically minimized with an OPLS4 force field by 2D sketcher and Ligprep tool of Maestro. Hydrogen atoms and missing side chains were added and optimized, waters within 5 Å of the co-crystallized ligand were removed, and the structures were minimized using the OPLS4 force field to relieve any steric clashes and optimize hydrogen-bonding networks.

In protein–protein docking, Ca^{2+}/CaM or TFP-bound Ca^{2+}/CaM and the SOAR domain were considered as the ligand and receptor, respectively. PIPER pose score was utilized to calculate the interaction energy between proteins via the PIPER program of Maestro.

2.8 | Statistical Analysis

Outliers were identified before performing a *t*-test or two-way ANOVA using the robust regression and outlier removal (ROUT) method ($Q = 1\%$). An unpaired *t*-test and one-sample *t*-test were used to determine differences between the groups or with theoretical value, respectively. Otherwise, a two-way ANOVA was used. The significance level is represented by asterisks (*$p < 0.05$, **$p < 0.01$, ***$p < 0.001$, ****$p < 0.0001$; non-significance shown as ns). GraphPad Prism 10.2.3 (GraphPad Software, USA) was used for data analysis and plotting. The mean value, standard deviation, and group size were mentioned in the results of the manuscript.

3 | Results

3.1 | TFP Induces Sustained Ca^{2+} Elevation in Primary Astrocytes With Biphasic Concentration Dependency

To investigate whether cultured astrocytes exhibit TFP-induced Ca^{2+} signals comparable to those observed in U87MG cells, we treated primary cortical astrocytes with TFP. We found a

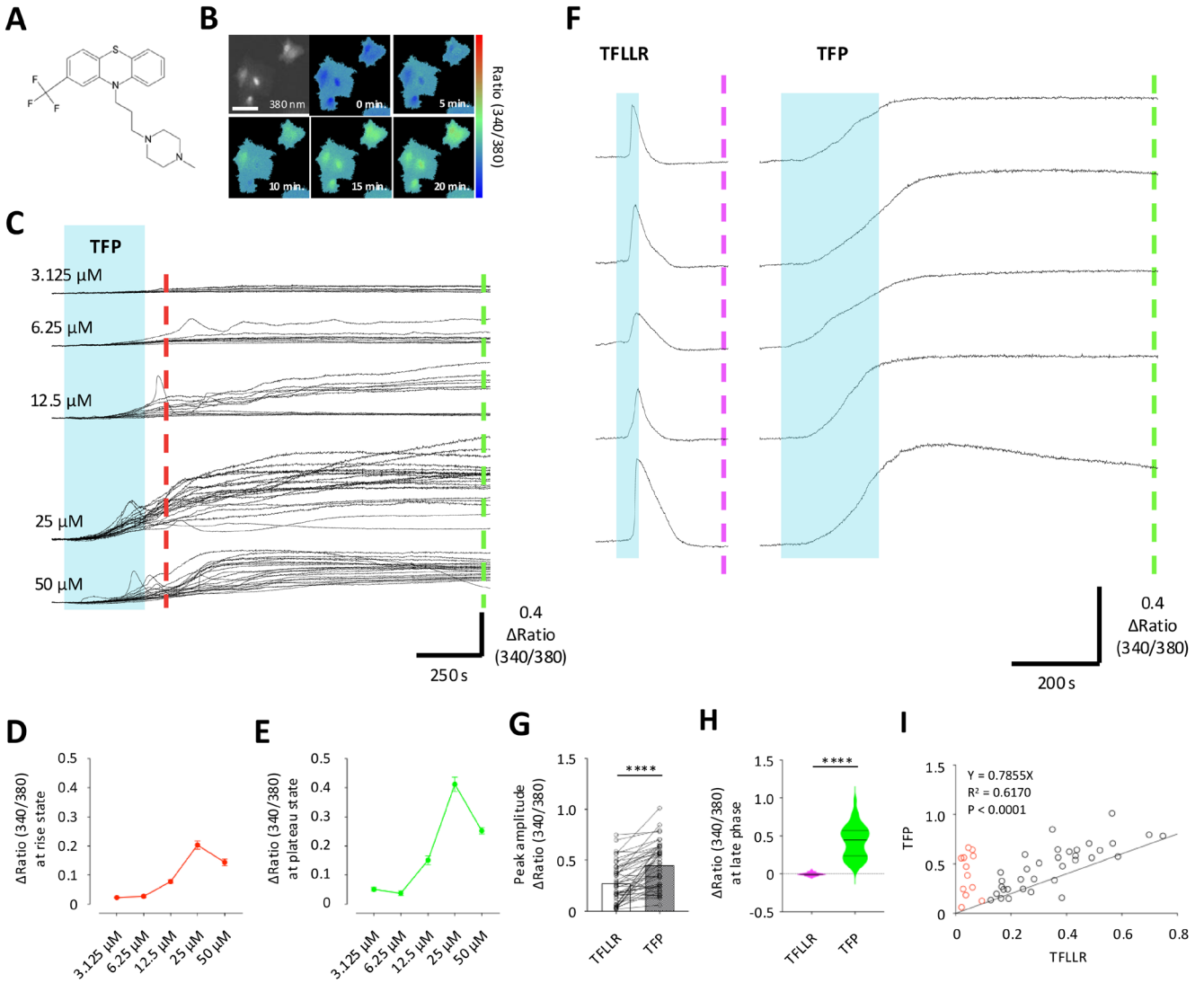

FIGURE 1 | TFP-induced Ca^{2+} elevation in astrocytes shows biphasic concentration dependence and differential kinetics. (A) Skeletal formula of trifluoperazine. (B) Left top, Fura-2AM loaded cells. From right top, representative Ca^{2+} imaging 340/380 ratio images taken at baseline 5, 10, 15, and 20 min. Scale bar = 100 μm. (C) Ca^{2+} signal traces of TFP 3.125, 6.25, 12.5, 25, and 50 μM treated primary astrocyte culture. (D) Dose–response graph of amplitude of Ca^{2+} signals at rise phase (error bar: S.e.m.). (E) Dose–response graph of amplitude Ca^{2+} signals at plateau phase (error bar: S.e.m.). (F) Ca^{2+} signal traces of TFLLR 30 μM (left) and TFP 12.5 μM (right) treated conditions. (G) Peak amplitude of Ca^{2+} signals of TFLLR- or TFP-treated conditions (paired *t*-test, ****$p < 0.0001$). (H) Amplitude at late phase of TFLLR- or TFP-treated conditions (paired *t*-test, ****$p < 0.0001$). (I) Correlation between peak amplitude of Ca^{2+} signals of TFLLR- or TFP-treated conditions (linear regression, $p < 0.0001$).

sustained increase in cytosolic Ca^{2+} levels, similar to the response observed in U87MG cells (Figure 1B,C). Since high concentrations of TFP can induce cell death, it was necessary to determine an appropriate TFP concentration that would allow for mechanistic investigation without cytotoxic effects. To determine the concentration dependence of the responses in primary astrocyte cultures, we treated cells with five TFP concentrations (3.125, 6.25, 12.5, 25, and 50 μM). For analysis, we measured TFP-induced Ca^{2+} signals at two different time points. As previously reported, inositol phosphate 3 receptor (IP3R) is involved in TFP-induced Ca^{2+} elevation. However, TFP-induced Ca^{2+} elevation shows a plateau, which is an outside chance to be mediated by IP3R solely, so we hypothesized that there is another Ca^{2+} source for the sustained Ca^{2+} signals. Thus, Ca^{2+} signals were measured at two distinct time points: the initial rise phase (red dotted line) and the plateau phase (green dotted line) (Figure 1D,E).

Our analysis revealed that TFP-induced Ca^{2+} signals increased dose-dependently from 3.125 to 25 μM but decreased at 50 μM in both the rise and plateau phases (Ca^{2+} signals at rise, 3.125 μM: mean = 0.02303, SD = 0.01465, $n = 34$, four coverslips; 6.25 μM: mean = 0.03177, SD = 0.0215, $n = 17$, two coverslips; 12.5 μM: mean = 0.08081, SD = 0.051107, $n = 59$, five coverslips; 25 μM: mean = 0.2033, SD = 0.1062, $n = 52$, four coverslips; 50 μM: mean = 0.1437, SD = 0.08702, $n = 56$, 3 coverslips) and plateau (Ca^{2+} signals at plateau, 3.125 μM: mean = 0.05147, SD = 0.03421, $n = 34$, four coverslips; 6.25 μM: mean = 0.0483, SD = 0.05130, $n = 17$, two coverslips; 12.5 μM: mean = 0.1509, SD = 0.1164, $n = 59$, five coverslips; 25 μM: mean = 0.4115, SD = 0.181, $n = 52$, four coverslips; 50 μM: mean = 0.2524, SD = 0.08356, $n = 56$, three coverslips). At 50 μM, some cells exhibited morphological changes such as shrinkage and the appearance of cytoplasmic vesicles (data not shown) (Figure 1C–E). Based on these results and previous reports,

we selected 12.5 μM as the optimal concentration for subsequent experiments. This concentration not only elicited robust Ca^{2+} responses without overt toxicity on astrocytes but also aligned with pharmacologically relevant doses. Prior studies have shown that approximately 12.5 μM TFP is effective across diverse human tumor cell lines (Feng et al. 2018; Kang et al. 2017; Xia et al. 2019; Yeh et al. 2012). Taken together, our findings demonstrate that TFP induces Ca^{2+} signals in astrocytes and that TFP-induced Ca^{2+} elevation in astrocytes exhibits biphasic concentration dependency.

3.2 | TFP Exhibits Distinct Ca^{2+} Signal Kinetics

To further investigate the kinetics of TFP-induced Ca^{2+} signaling, we compared it to TFLLR-NH_2 (TFLLR), a PAR1 agonist that activates $G_{\alpha q}$-coupled GPCRs and induces IP3R-dependent Ca^{2+} signaling (Garavilla et al. 2001; Han et al. 2011; Lee et al. 2007). To directly compare TFLLR- and TFP-induced Ca^{2+} signals in individual cells, TFLLR (30 μM) was applied after a 60-s baseline recording, followed by Ca^{2+} signal measurement. After a 10-min interval for Ca^{2+} restoration in the ER, TFP (12.5 μM) was applied, and the TFP-induced Ca^{2+} signals were recorded in the same cells. TFLLR treatment elicited a rapid peak followed by a gradual decay, whereas TFP treatment resulted in a slower onset with sustained Ca^{2+} elevation (Figure 1F). The peak amplitude of TFP-induced Ca^{2+} signals (mean = 0.4509, SD = 0.2253, n = 46, four coverslips) was significantly higher than that of TFLLR-induced signals (mean = 0.2708, SD = 0.1957, n = 46, four coverslips) (Figure 1G). Furthermore, while TFLLR-induced signals returned to near-baseline levels (mean = −0.0022, SD = 0.0273, n = 46, four coverslips), TFP-induced signals remained elevated (mean = 0.4273, SD = 0.2155, n = 46, four coverslips) (Figure 1H).

Notably, some astrocytes did not respond to TFLLR, whereas all astrocytes responded to TFP, suggesting that TFP affects common Ca^{2+} signaling pathways. These findings highlight the distinct kinetics of TFP-mediated Ca^{2+} signaling. Furthermore, since ER Ca^{2+} release has been implicated in TFP-induced Ca^{2+} signals, we investigated the correlation between TFLLR- and TFP-induced peak amplitudes in TFLLR-responsive astrocytes. A positive correlation was observed (Figure 1I), suggesting that ER Ca^{2+} release influences the magnitude of TFP-induced Ca^{2+} signals.

3.3 | Extracellular Ca^{2+} Influx Is Essential for Sustained TFP-Induced Ca^{2+} Signals

Next, we investigated the source of Ca^{2+} contributing to the plateau phase of TFP-induced Ca^{2+} signal. As previously mentioned, TFP-induced Ca^{2+} signals in the U87MG cell line were affected by Ca^{2+}-free solution containing ethylene glycol-bis-*N*,*N*,*N*′,*N*′-tetraacetic acid (EGTA) (Kang et al. 2017). In astrocytes, the plateau phase of TFP-induced Ca^{2+} signals persisted for over 10 min, suggesting a reliance on extracellular Ca^{2+} influx, given the limited capacity of intracellular Ca^{2+} stores. To test this hypothesis, Ca^{2+} imaging was performed under normal conditions (2 mM Ca^{2+} solution) and in a Ca^{2+}-free solution containing EGTA (200 nM), a Ca^{2+} chelating agent. Astrocytes were preincubated with Fura 2-AM in a 2 mM Ca^{2+} solution, and Ca^{2+}-free solution was introduced at the start of imaging. Following a 60-s baseline recording, TFP was applied in the Ca^{2+}-free solution. In contrast to the sustained Ca^{2+} elevation observed in the 2 mM Ca^{2+} condition, TFP treatment in Ca^{2+}-free solution resulted in an initial transient increase but failed to maintain a prolonged response (Figure 2A).

Comparison of Ca^{2+} signals at the rise and plateau phases revealed a significant difference in the rise phase between conditions (2 mM Ca^{2+}: mean = 0.095, SD = 0.087, n = 44, three coverslips; Ca^{2+}-free: mean = 0.058, SD = 0.074, n = 58, five coverslips). During the plateau phase, Ca^{2+} signals were significantly decreased in the Ca^{2+}-free condition (2 mM Ca^{2+}: mean = 0.207, SD = 0.198, n = 44, three coverslips; Ca^{2+}-free: mean = 0.018, SD = 0.060, n = 58, five coverslips) (Figure 2B). When we calculated the difference between the rise and plateau phases (ΔΔRatio), the value for the 2 mM Ca^{2+} condition (mean = 0.1122, SD = 0.1569, n = 44, three coverslips) was significantly greater than that of the Ca^{2+}-free condition (mean = −0.4032, SD = 0.08508, n = 58, five coverslips) (Figure 2C). These results indicate that extracellular Ca^{2+} influx is essential for sustaining the plateau phase of TFP-induced Ca^{2+} signals.

3.4 | TFP-Induced Ca^{2+} Plateau Phase Is Calmodulin-Dependent

TFP is known to bind to Ca^{2+}-bound calmodulin (Ca^{2+}/CaM) and inhibit its enzymatic activity. Previously, gene silencing of CaM2 reduced TFP-induced Ca^{2+} signals in U87MG cells (Kang et al. 2017). To assess the role of CaM in the plateau phase of TFP-induced Ca^{2+} signals, we used W-7 dichloride, a CaM inhibitor (Figure 2D). After establishing a baseline, W-7 (10 μM) was applied for 2 min, followed by TFP treatment in the presence of W-7. Ca^{2+} signals were analyzed at two time points: 300 s after TFP application (rise phase) and 1000 s after TFP application (plateau phase).

Interestingly, W-7 treatment had no effect on the rise phase of TFP-induced Ca^{2+} signals (TFP only: mean = 0.04464, SD = 0.02342, n = 16, four coverslips; W-7 + TFP: mean = 0.04284, SD = 0.01858, n = 13, three coverslips). However, during the plateau phase, Ca^{2+} signals were significantly reduced in W-7-treated cells compared to vehicle-treated controls (TFP only: mean = 0.1354, SD = 0.08240, n = 16, four coverslips; W-7 + TFP: mean = 0.03477, SD = 0.02285, n = 13, three coverslips) (Figure 2E,F). Furthermore, when comparing the difference between the rise and plateau phases, Ca^{2+} signals in the W-7 + TFP condition were near zero, whereas the TFP-only condition maintained a positive signal (TFP only: mean = 0.09073, SD = 0.07161, n = 16, four coverslips; W-7 + TFP: mean = −0.008069, SD = 0.02737, n = 13, three coverslips) (Figure 2G). These findings suggest that the plateau phase of TFP-induced Ca^{2+} elevation is CaM-dependent.

3.5 | The STIM1–Orai Complex Mediates TFP-Induced Ca^{2+} Elevation

We demonstrated that the plateau phase of the TFP-induced Ca^{2+} signal originates from extracellular Ca^{2+}, implying the involvement of Ca^{2+} channels or transporters. In cells, extracellular Ca^{2+} entry occurs through various mechanisms, including

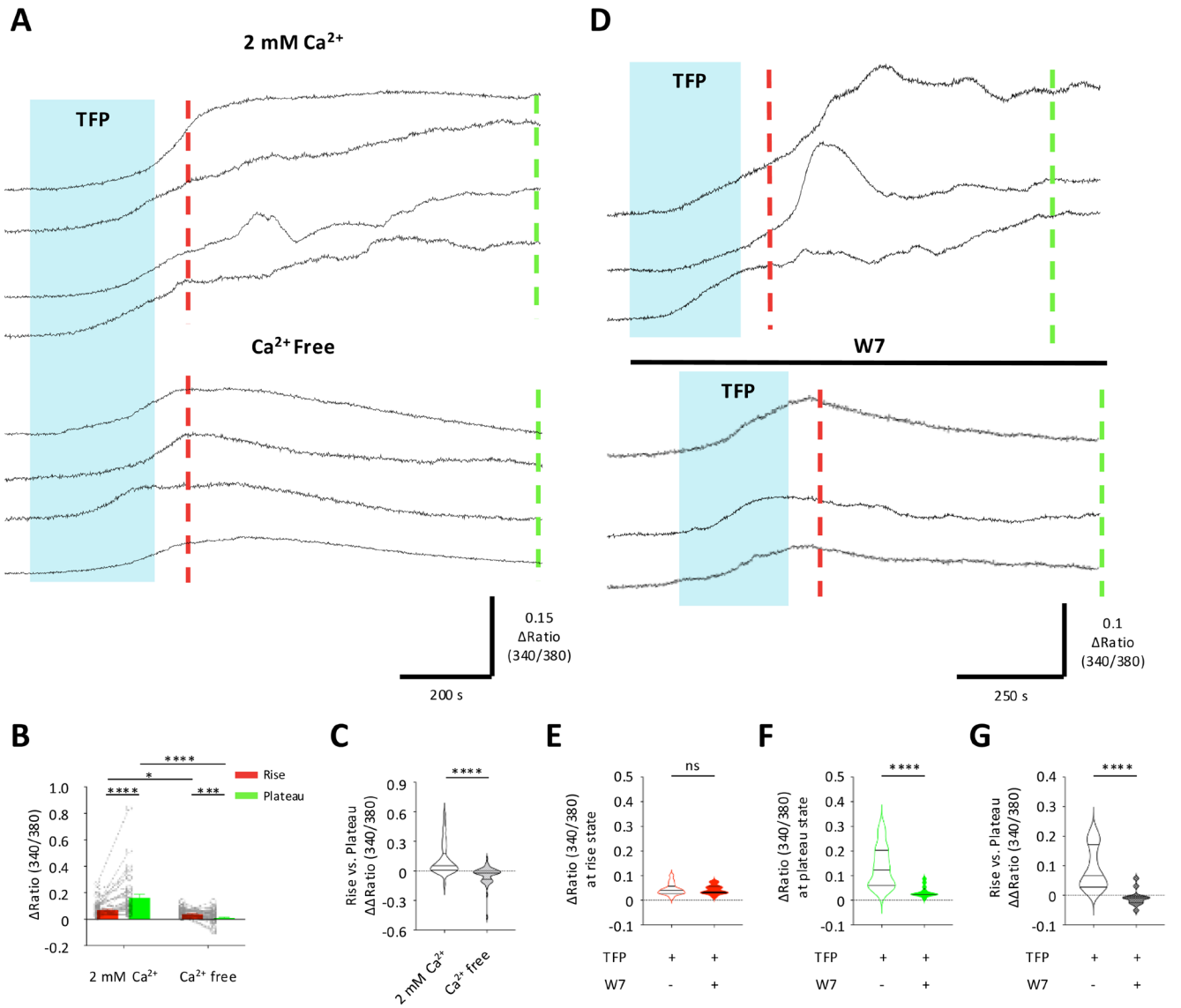

FIGURE 2 | Ca^{2+} entry and calmodulin are necessary for sustained TFP-induced Ca^{2+} elevation. (A) Ca^{2+} signal traces induced by TFP in 2 mM Ca^{2+} or Ca^{2+}-free conditions. (B) Ca^{2+} signal amplitude at rise (red) and plateau (green) phase (error bar: S.e.m., in group, paired *t*-test, $^{***}p < 0.001$, $^{****}p < 0.0001$, between group, unpaired *t*-test, $^{*}p < 0.05$, $^{****}p < 0.0001$). (C) Amplitude difference between rise and plateau phase (unpaired *t*-test, $^{****}p < 0.0001$). (D) Ca^{2+} signal traces induced by TFP in vehicle or W-7 10 μM conditions. (E) Ca^{2+} signal amplitude at rise phase (unpaired *t*-test, $^{ns}p > 0.05$). (F) Ca^{2+} signal amplitude at plateau phase (unpaired *t*-test, $^{****}p < 0.0001$). (G) Amplitude difference between rise and plateau phase (unpaired *t*-test, $^{****}p < 0.0001$).

voltage-dependent Ca^{2+} channels, agonist-dependent Ca^{2+} channels, Na^{+}/Ca^{2+} exchangers, and Ca^{2+}-release-activated channels (Clapham 2007). The rise phase of the TFP-induced Ca^{2+} signal was independent of extracellular Ca^{2+}, and previous studies have shown that TFP depletes ER Ca^{2+} stores in U87MG cells, suggesting ER involvement. Store-operated Ca^{2+} entry (SOCE), mediated by the STIM1–Orai/TRPC complex, replenishes ER Ca^{2+} following IP3R activation (Prakriya and Lewis 2015). Notably, SOCE desensitization is Ca^{2+}/CaM-dependent (Li et al. 2017). Based on these findings, we hypothesized that TFP inhibits SOCE desensitization by binding to Ca^{2+}/CaM, thereby sustaining Ca^{2+} influx. In a previous study, we identified the STIM1–Orai complex as astrocyte's predominant SOCE machinery (Kwon et al. 2017). Therefore, we investigated its involvement in TFP-induced Ca^{2+} elevation.

To determine whether SOCE mediates the plateau phase of TFP-induced Ca^{2+} signals, we performed gene silencing of the STIM1–Orai complex (STIM1, Orai1, Orai2, and Orai3) in astrocytes. First, we knocked down *Stim1*, the key initiator of SOCE that senses ER Ca^{2+} levels, and recorded Ca^{2+} signals. Gene silencing of *Stim1* significantly reduced Ca^{2+} signals in both the rise (scrambled shRNA: mean = 0.1937, SD = 0.07089, $n = 17$, seven coverslips; *Stim1* shRNA: mean = 0.1082, SD = 0.06798, $n = 21$, 12 coverslips) and plateau phases (scrambled shRNA: mean = 0.3989, SD = 0.1414, $n = 17$, seven coverslips; *Stim1* shRNA: mean = 0.2284, SD = 0.1558, $n = 21$, 12 coverslips) (Figure 3A–C). Furthermore, when comparing the difference between the rise and plateau phases, gene silencing of Stim1 showed less positive signal than the scrambled shRNA-treated condition (scrambled shRNA: mean = 0.2052, SD = 0.1203,

$n = 17$, seven coverslips; *Stim1* shRNA: mean = 0.1202, SD = 0.1158, $n = 21$, 12 coverslips) (Figure 3D).

Next, we knocked down Orai1–3, which form the SOCE channel. Gene silencing of Orai1 significantly reduced Ca^{2+} signals in both the rise (scrambled shRNA: mean = 0.1669, SD = 0.08045, $n = 8$, four coverslips; *Orai1* shRNA: mean = 0.04630, SD = 0.02529, $n = 8$, three coverslips) and plateau phases (scrambled shRNA: mean = 0.2831, SD = 0.1656, $n = 8$, four coverslips; *Orai1* shRNA: mean = 0.03290, SD = 0.02186, $n = 8$, three coverslips) (Figure 3E–G). The difference between the rise and plateau phases was reduced to near zero by gene silencing of *Orai1* (scrambled shRNA: mean = 0.1162, SD = 0.09688, $n = 8$, four coverslips; *Orai1* shRNA: mean = −0.0134, SD = 0.01174, $n = 8$, three coverslips) (Figure 3H). Gene silencing of *Orai2* or *Orai3* also significantly reduced Ca^{2+} signals in the plateau phase (scrambled shRNA: mean = 0.1187, SD = 0.03732, $n = 7$, two coverslips; *Orai2* shRNA: mean = 0.06973, SD = 0.04527, $n = 11$, two coverslips; *Orai3* shRNA: mean = 0.04562, SD = 0.03119, $n = 9$, three coverslips). However, not *Orai2*, only *Orai3* knockdown showed a tendency to decrease Ca^{2+} signals in the rise phase (scrambled shRNA: mean = 0.06829, SD = 0.03231, $n = 7$, two coverslips; *Orai2* shRNA: mean = 0.05195, SD = 0.02744, $n = 11$, two coverslips; *Orai3* shRNA: mean = 0.04407, SD = 0.01886, $n = 9$, three coverslips) (Figure 3I–O). Similarly, gene silencing of *Orai3* significantly reduced the difference between the rise and plateau phases, but gene silencing of *Orai2* showed a tendency to decrease (scrambled shRNA: mean = 0.05037, SD = 0.04285, $n = 7$, two coverslips; *Orai2* shRNA: mean = 0.01778, SD = 0.04045, $n = 11$, two coverslips; *Orai3* shRNA: mean = −0.007689, SD = 0.0234, $n = 9$, three coverslips) (Figure 3P). These results indicate that the STIM1–Orai complex is involved in TFP-induced Ca^{2+} elevation.

3.6 | TFP Prevents SOCE Desensitization

To restore Ca^{2+} in the ER, STIM1 in the ER membrane senses the decreased Ca^{2+} concentration and interacts with Orai channels in the plasma membrane to form the STIM1–Orai complex. This complex allows extracellular Ca^{2+} to enter the cytosol (Verkhratsky and Parpura 2014). Elevated intracellular Ca^{2+} levels then trigger Ca^{2+}-dependent inactivation (CDI) of SOCE through the dissociation of the STIM1–Orai complex in a Ca^{2+}/CaM-dependent manner (Li et al. 2017). Based on this mechanism, we hypothesized that TFP sustains SOCE activity by inhibiting CDI via Ca^{2+}/CaM inhibition. To test this, we employed a Ca^{2+} imaging protocol to measure SOCE in astrocytes (Kwon et al. 2017). Astrocytes were initially placed in Ca^{2+}-free solution, and thapsigargin (1 μM) was applied to deplete ER Ca^{2+} stores. After stabilization of the baseline signal, 2 mM Ca^{2+} was reintroduced to induce SOCE. TFP was administered 100 s prior to Ca^{2+} reintroduction to assess its effect on SOCE desensitization (Figure 4A). Thapsigargin-induced Ca^{2+} signals prior to Ca^{2+} reintroduction were comparable between control and TFP-treated groups (2 mM Ca^{2+}: mean = 0.1562, SD = 0.105, $n = 32$, two coverslips; TFP + 2 mM Ca^{2+}: mean = 0.1516, SD = 0.07733, $n = 33$, two coverslips) (Figure 4B). To quantify desensitization, we measured Ca^{2+} signals at two time points (peak and decay) following Ca^{2+} reintroduction. There was no significant difference in peak or decay Ca^{2+} responses between the groups (2 mM Ca^{2+} at peak: mean = 0.170, SD = 0.070, $n = 32$; 2 mM Ca^{2+} at decay: mean = 0.154, SD = 0.058, $n = 32$, two coverslips; TFP + 2 mM Ca^{2+} at peak: mean = 0.151, SD = 0.071, $n = 33$; TFP + 2 mM Ca^{2+} at decay: mean = 0.173, SD = 0.045, $n = 33$, two coverslips) (Figure 4C).

To evaluate SOCE desensitization on a per-cell basis, we calculated the desensitization index as the ratio of the Ca^{2+} signal at decay to the peak. In the control group, this ratio was less than 1, indicating typical CDI after Ca^{2+} influx. In contrast, TFP significantly increased the desensitization index above 1, suggesting a lack of signal decay (2 mM Ca^{2+}: mean = 0.9291, SD = 0.1786, $n = 32$, two coverslips; TFP + 2 mM Ca^{2+}: mean = 1.344, SD = 0.5502, $n = 33$, two coverslips) (Figure 4D). This indicates that TFP abolished the decay phase of the Ca^{2+} signal, resulting in sustained SOCE activity. Together, these results suggest that TFP prevents SOCE desensitization, likely by inhibiting the Ca^{2+}/CaM-mediated CDI mechanism, thereby maintaining prolonged Ca^{2+} influx in astrocytes.

3.7 | TFP Induces Sustained Ca^{2+} Elevation in Astrocytes of Acute Hippocampal Brain Slices

Given that primary astrocyte cultures differ significantly from in vivo astrocytes in morphology, gene expression, and function, we sought to determine whether TFP elicits similar effects in a more physiologically relevant context. To test whether TFP induces sustained Ca^{2+} elevation in brain tissue, we performed whole-cell patch-clamp recordings from astrocytes in the dentate gyrus (DG) of acute hippocampal slices. Calcium Green-1 dextran, a fluorescent calcium indicator, was delivered through the patch pipette to enable real-time Ca^{2+} imaging (Figure 5A). To confirm that the patched cells were astrocytes, we assessed passive membrane properties. Patched cells displayed linear current–voltage (*I–V*) relationships (Figure 5B), consistent with passive conductance typical of astrocytes. The rectification index did not significantly differ from the theoretical value of 1 (mean = 0.9326, SD = 0.3982, $n = 8$) and the resting membrane potential was hyperpolarized, closely matching the expected astrocytic value of −80 mV (mean = −81.09, SD = 3.491, $n = 8$) (Figure 5C).

Ten minutes after whole-cell configuration (allowing dye diffusion), Ca^{2+} signals were recorded (Figure 5A). Following 4 min of baseline recording, TFP (12.5 μM) was administered by bath application. Consistent with results from primary cultures, TFP induced a sustained Ca^{2+} elevation in DG astrocytes (Figure 5D). The Ca^{2+} signal during the plateau phase was significantly greater than during the initial rise phase (rise: mean = 4.109, SD = 5.713, $n = 8$; plateau: mean = 11.65, SD = 11.23, $n = 8$) (Figure 5E). Furthermore, the difference between plateau and rise phases was significantly greater than zero (mean = 7.542, SD = 5.572, $n = 8$), confirming a sustained response (Figure 5F). Together, these results demonstrate that TFP induces prolonged Ca^{2+} elevation not only in primary cultured astrocytes, but also in astrocytes within acute hippocampal slices, supporting the physiological relevance of TFP's effects on astrocytic Ca^{2+} dynamics.

3.8 | TFP Disrupts Ca^{2+}/CaM-STIM1 Interaction

A well-characterized mechanism underlying CDI of SOCE involves the interaction between Ca^{2+}/CaM and the SOAR domain

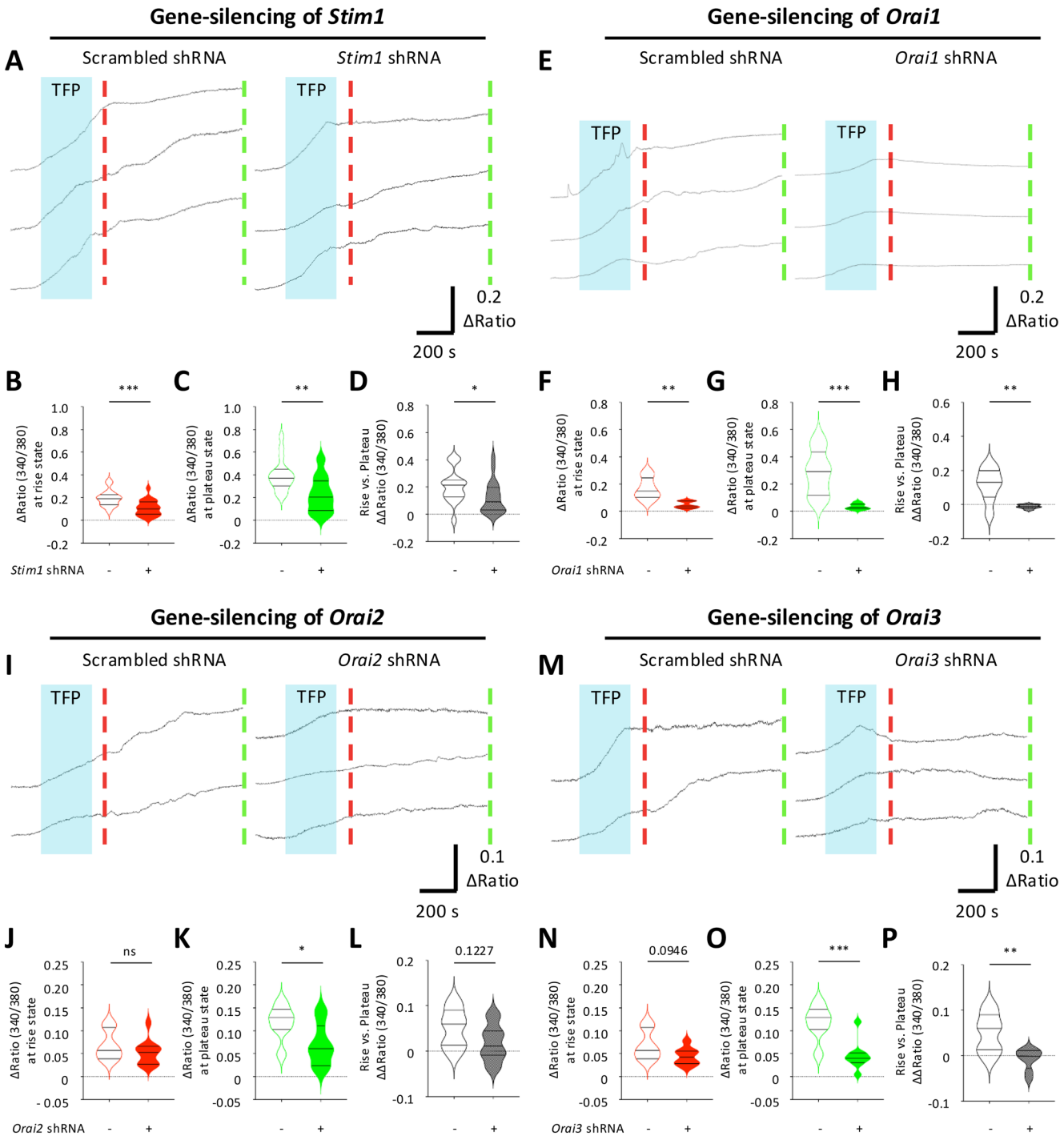

FIGURE 3 | Gene silencing of STIM1–Orai complex in astrocytes reduces TFP-induced Ca^{2+} elevation. (A) Ca^{2+} signal traces induced by TFP in scrambled or Stim1 shRNA conditions. (B) Ca^{2+} signal amplitude at rise phase (unpaired *t*-test, $^{***}p < 0.001$). (C) Ca^{2+} signal amplitude at plateau phase (unpaired *t*-test, $^{**}p < 0.01$). (D) Amplitude difference between rise and plateau phase (unpaired *t*-test, $^{*}p < 0.05$). (E) Ca^{2+} signal traces induced by TFP in scrambled or *Orai1* shRNA conditions. (F) Ca^{2+} signal amplitude at rise phase (unpaired *t*-test, $^{**}p < 0.01$). (G) Ca^{2+} signal amplitude at plateau phase (unpaired *t*-test, $^{***}p < 0.001$). (H) Amplitude difference between rise and plateau phase (unpaired *t*-test, $^{**}p < 0.01$). (I) Ca^{2+} signal traces induced by TFP in scrambled or Orai2 shRNA conditions. (J) Ca^{2+} signal amplitude at rise phase (unpaired *t*-test, $^{ns}p > 0.05$). (K) Ca^{2+} signal amplitude at plateau phase (unpaired *t*-test, $^{*}p < 0.05$). (L) Amplitude difference between rise and plateau phase (unpaired *t*-test, $p = 0.1227$). (M) Ca^{2+} signal traces induced by TFP in scrambled or *Orai3* shRNA conditions. (N) Ca^{2+} signal amplitude at rise phase (unpaired *t*-test, $p = 0.0946$). (O) Ca^{2+} signal amplitude at plateau phase (unpaired *t*-test, $^{***}p < 0.001$). (P) Amplitude difference between rise and plateau phase (unpaired *t*-test, $^{**}p < 0.01$).

of STIM1, which leads to the dissociation of the STIM1–Orai complex (Li et al. 2017). We hypothesized that TFP prevents SOCE desensitization by disrupting this Ca^{2+}/CaM–STIM1 interaction. To test this hypothesis, we performed in silico protein–protein docking simulations using the PIPER module in Maestro. The 3D structures of Ca^{2+}/CaM, TFP-bound Ca^{2+}/

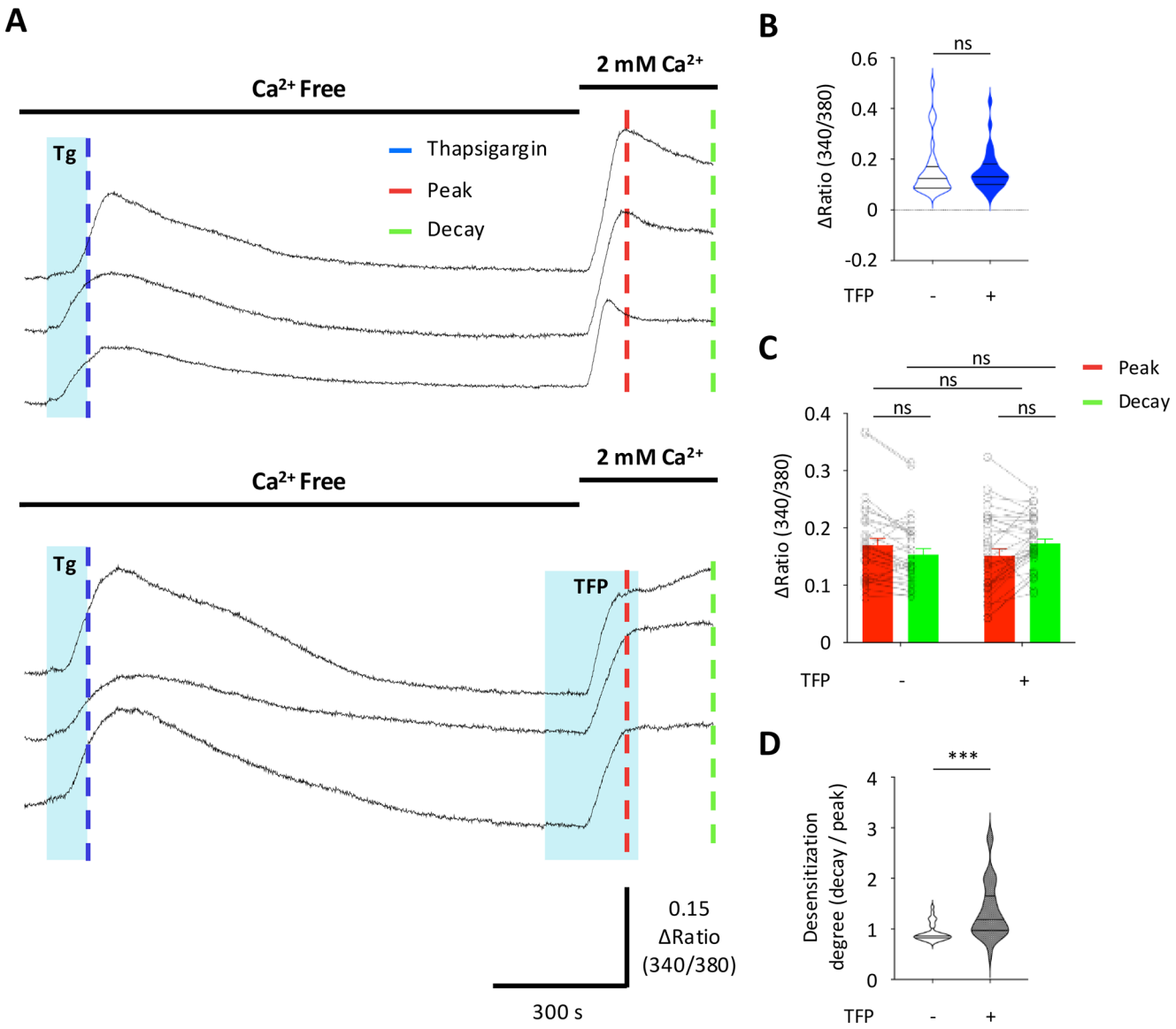

FIGURE 4 | TFP blocks SOCE desensitization kinetics. (A) Ca^{2+} signal traces of thapsigargin and SOCE in vehicle or TFP pre-treated conditions. (B) Amplitude of Ca^{2+} signals induced by thapsigargin (unpaired *t*-test, $^{ns}p > 0.05$). (C) Amplitude of Ca^{2+} signals at peak (red) and decay (green) (error bar: S.e.m., in group, paired *t*-test, $^{ns}p > 0.05$, between group, unpaired *t*-test, $^{ns}p > 0.05$). (D) Desensitization index (decay/peak) (unpaired *t*-test, $^{***}p < 0.001$).

CaM, and the SOAR domain of STIM1 were retrieved from the Protein Data Bank and preprocessed using Maestro's Protein Preparation Wizard. In the docking setup, Ca^{2+}/CaM or TFP-bound Ca^{2+}/CaM was defined as the ligand, and the SOAR domain as the receptor. The interaction strength was quantified using the PIPER pose score, where more negative values indicate more stable protein–protein interactions. Among the predicted models, we selected those in which binding occurred at residues L390–F391 of the SOAR domain, a region previously reported as a binding site of Ca^{2+}/CaM (Li et al. 2017). As expected, Ca^{2+}/CaM docked to the SOAR domain with a strong interaction score of −445.135. In contrast, the TFP-bound Ca^{2+}/CaM displayed a substantially weaker interaction with the SOAR domain, with a PIPER score of −134.643 (Figure 6B). This significant reduction in binding affinity suggests that TFP interferes with the Ca^{2+}/CaM–STIM1 interaction. These findings support the hypothesis that TFP disrupts this regulatory protein–protein interaction, thereby impairing CDI and promoting sustained activation of SOCE.

4 | Discussion

In this study, we investigated the molecular mechanism underlying sustained TFP-induced Ca^{2+} elevation in astrocytes. We first examined the concentration dependency and kinetics of TFP-induced Ca^{2+} signals (Figure 1). We then found that extracellular Ca^{2+} and CaM are necessary for the plateau phase of TFP-induced Ca^{2+} elevation (Figure 2). Using gene silencing with shRNA targeting SOCE-related genes, we demonstrated that the STIM1–Orai complex is involved in TFP-induced Ca^{2+} elevation (Figure 3). Finally, we assessed the effect of TFP on the SOCE system and

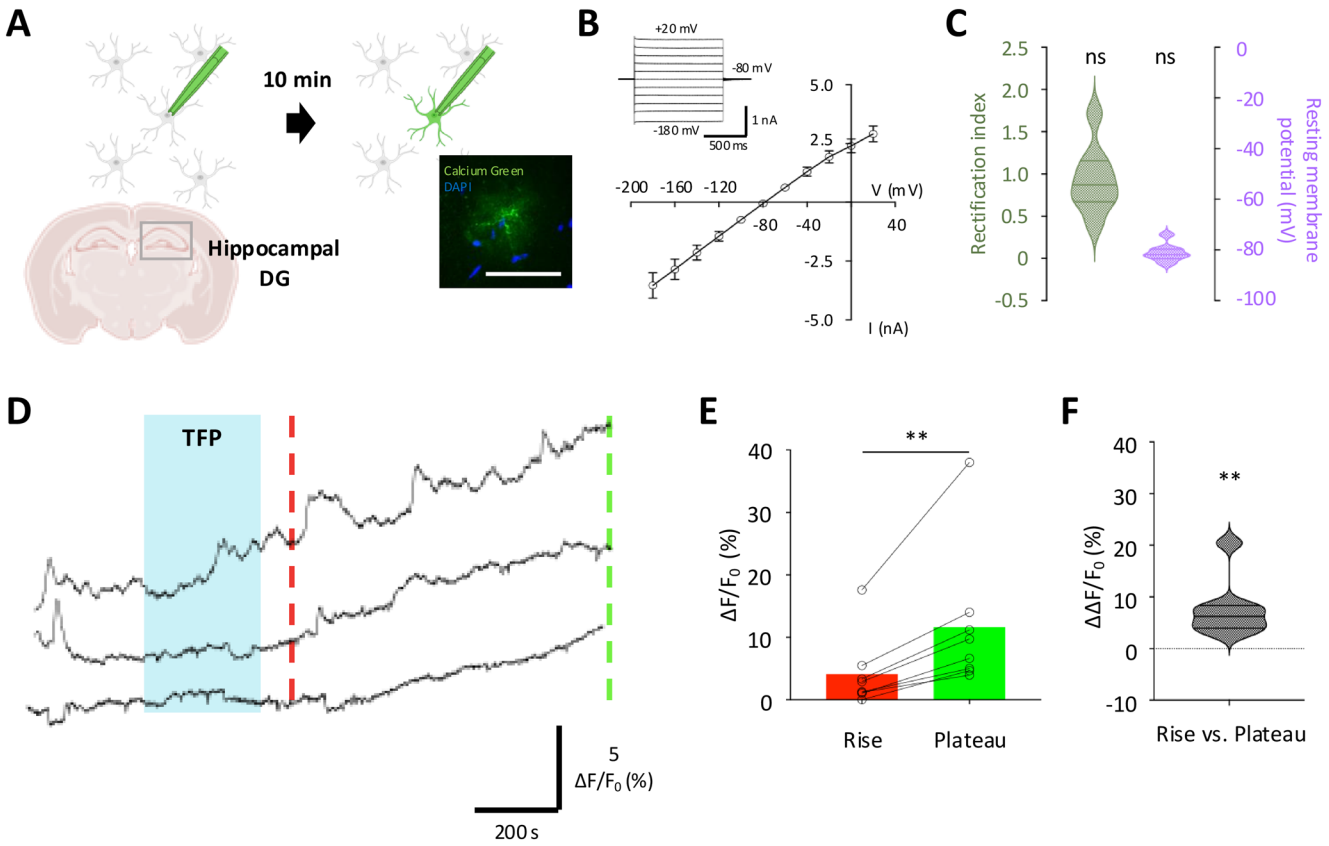

FIGURE 5 | TFP induces sustained Ca^{2+} elevation in astrocytes ex vivo. (A) Experimental diagram for Ca^{2+} imaging of hippocampal dentate gyrus astrocytes. Scale bar = 50 μm. (B) Representative passive conductance, measured at voltages ranging from −180 to +20 mV in 20 mV step increments, and *I–V* curve showing passive conductance, with current responses to voltage steps. (C) Rectification index, calculated as the difference in current between +20 and −80 mV, divided by the difference between −80 and −180 mV (one-sample *t*-test, theoretical mean = 1, $^{ns}p < 0.05$) and resting membrane potential (mV) of hippocampal dentate gyrus astrocytes (One-sample *t*-test, theoretical mean = −80, $^{ns}p < 0.05$). (D) Ca^{2+} signal traces induced by TFP. (E) Ca^{2+} signal amplitude at rise (red) and plateau (green) phase (paired *t*-test, $^{**}p < 0.01$). (F) Amplitude difference between rise and plateau phase (one-sample *t*-test, theoretical mean = 0, $^{**}p < 0.01$).

found that TFP locks SOCE channels open by inhibiting Ca^{2+}/CaM-dependent desensitization (Figure 4). Additionally, we confirmed the reproducibility of this phenomenon in hippocampal dentate gyrus astrocytes ex vivo, demonstrating its physiological relevance beyond cultured cells (Figure 5). Collectively, these findings demonstrate that TFP induces sustained Ca^{2+} signals by preventing SOCE channel desensitization by preventing Ca^{2+}/CaM-dependent desensitization (Figure 6).

TFP-induced Ca^{2+} elevation exhibited distinct kinetics compared to GPCR-mediated Ca^{2+} release in astrocytes. TFP-induced Ca^{2+} elevation displayed slow-rising kinetics, requiring more than 5 min to reach a plateau and resulting in a prolonged, elevated Ca^{2+} level without a decay (Figure 1A). Due to these unique kinetics, the peak amplitudes of TFP-induced Ca^{2+} signals were almost equivalent to Ca^{2+} signals observed during the late plateau phase (Figure 1G,H). Interestingly, the peak amplitude of TFP-induced Ca^{2+} signals showed a positive correlation with the peak amplitude of TFLLR-induced Ca^{2+} signals (Figure 1G,I). TFLLR-induced Ca^{2+} signals are characteristic of IP3R-mediated Ca^{2+} release from the ER. Our previous study demonstrated that TFP induces ER Ca^{2+} release by preventing IP3R inactivation (Kang et al. 2017). Therefore, the positive correlation between the peak amplitude of TFP- and TFLLR-induced Ca^{2+} signals suggests that ER Ca^{2+} release contributes to TFP-induced Ca^{2+} signals. Additionally, while a small subset of cells did not respond to TFLLR, nearly all astrocytes responded to TFP, further supporting that TFP-induced Ca^{2+} signals are mediated by ubiquitous Ca^{2+}-related molecules such as CaM. Sustained TFP-induced Ca^{2+} signals were abolished in the absence of extracellular Ca^{2+}. In Ca^{2+}-free conditions, TFP induced a transient increase in Ca^{2+} levels, followed by a decay to or below the baseline (Figure 2A). These results suggest that two differential Ca^{2+} sources contribute to TFP-induced Ca^{2+} signals: the rising phase originating from intracellular Ca^{2+} stores (e.g., ER) and the plateau phase relying on extracellular Ca^{2+} entry.

Interestingly, unlike TFP, another CaM inhibitor, W-7, did not affect ER Ca^{2+} release (rising phase), whereas W-7 inhibited extracellular Ca^{2+} entry (plateau phase), similar to TFP-induced Ca^{2+} signals in Ca^{2+}-free conditions (Figure 2D–G). Our previous study demonstrated that TFP-induced Ca^{2+} release occurs via IP3R disinhibition through Ca^{2+}/CaM blockade, whereas W-7 had no effect on the rising phase (Kang et al. 2017). This discrepancy could be due to Apo-CaM functioning as an IP3R subunit, which prevents some CaM inhibitors from binding effectively (Taylor and Laude 2002). Additionally, W-7 and TFP interact with different Ca^{2+}/CaM binding sites, leading to distinct effects on IP3R activity (Osawa et al. 1999, 1998; Sasakura

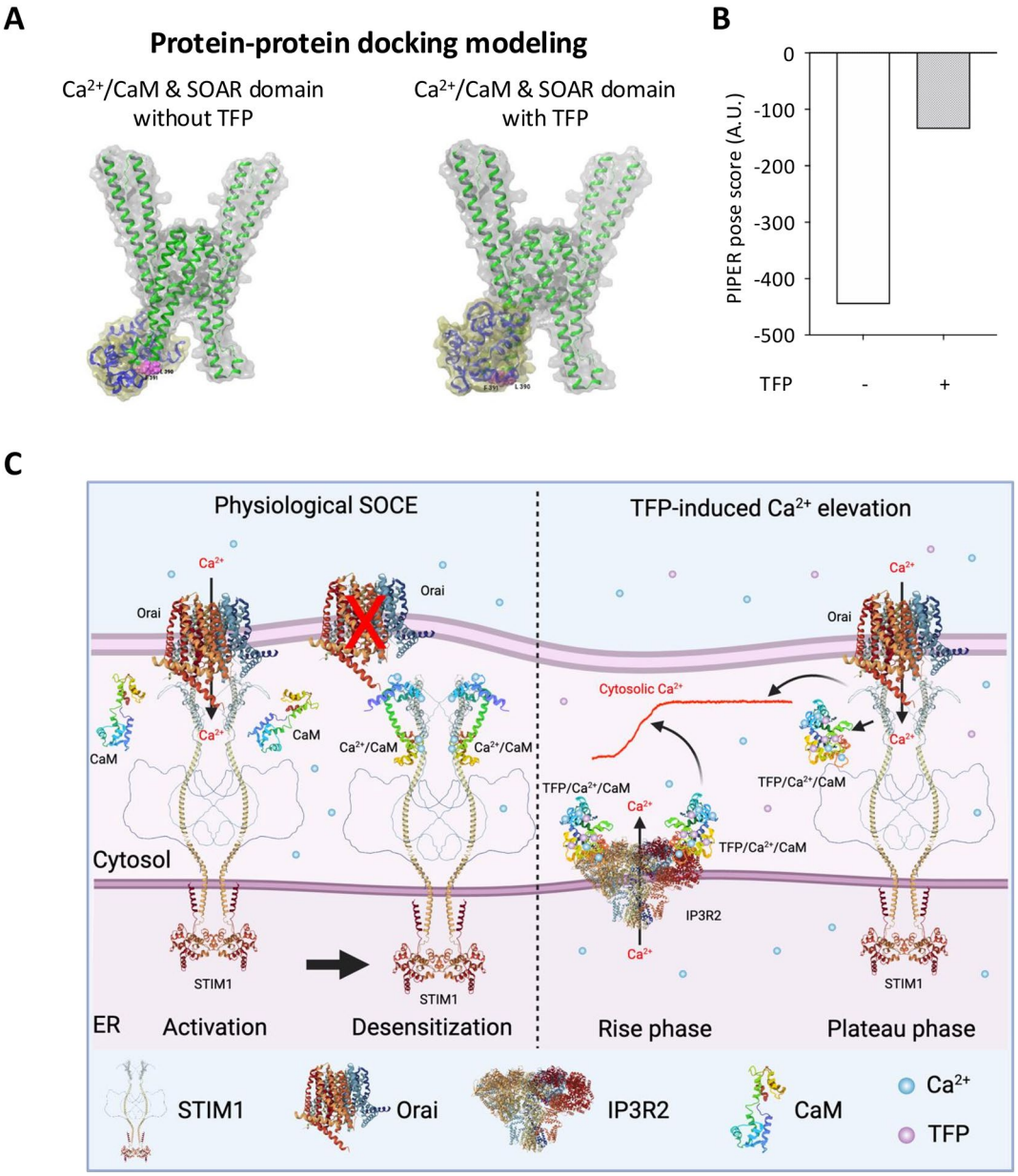

FIGURE 6 | TFP locks SOCE open by disrupting Ca^{2+}/CaM-STIM1 interaction. (A) Protein–protein docking model of Ca^{2+}/CaM and the SOAR domain of STIM1 without TFP and TFP, respectively. (B) PIPER pose score of protein–protein docking of Ca^{2+}/CaM and the SOAR domain of STIM1 without TFP and TFP, respectively. (C) SOCE is desensitized by Ca^{2+}/CaM in the physiological condition. TFP treatment induces ER Ca^{2+} release via disinhibition of IP3R2 and prolonged Ca^{2+} entry without a decay via inhibition of desensitization of SOCE. A schematic illustration is created in https://BioRender.com, and protein structures are from PDB and AlphaFold protein structure database (Hou et al. 2012; Kuboniwa et al. 1995; Schmitz et al. 2022; Vandonselaar et al. 1994; Wilson and Brunger 2000).

et al. 2012). If W-7 and TFP acted at the same binding site of Ca^{2+}/CaM, both W-7 and TFP should have induced sustained Ca^{2+} elevation in astrocytes. However, W-7 pre-treatment abolished the plateau phase of TFP-induced Ca^{2+} signals, indicating that although both inhibitors target Ca^{2+}/CaM, they may induce different conformational changes in its secondary structure. Therefore, TFP shows profoundly different response properties compared to W-7 and can be utilized for very different pharmacological approaches in which there is a need to induce and sustain a Ca^{2+} signal.

In astrocytes, TFP-induced Ca^{2+} release from the ER is followed by extracellular Ca^{2+} entry. This strongly suggests that SOCE is involved in the TFP-induced Ca^{2+} signal. To investigate this, we targeted four key genes—*Stim1*, *Orai1*, *Orai2*, and *Orai3*—using gene silencing. Knockdown of STIM1–Orai complex components significantly reduced TFP-induced Ca^{2+} signals (Figure 3). Among the Orai channels, gene silencing of Orai1 and Orai3 had a more pronounced effect than Orai2. Given that Orai1 and Orai3 are highly expressed in astrocytes and play significant roles in SOCE, our results align with both transcriptomic and functional evidence (Cahoy et al. 2008; Kwon et al. 2017; Zhang et al. 2014). Additionally, the knockdown of STIM1–Orai complex components also reduced the rising phase of TFP-induced Ca^{2+} signals. Our previous findings demonstrated that the rising phase is reduced in Ca^{2+}-free conditions,

implicating extracellular Ca^{2+} entry contributes to this rising phase (Kang et al. 2017). This further supports our conclusion that the SOCE system mediates TFP-induced Ca^{2+} signals. Collectively, our results indicate that Orai1 and Orai3 are the dominant CRAC channels mediating SOCE in astrocytes.

In astrocytes, Ca^{2+} serves as a key signaling molecule, regulating various biological processes and reflecting the degree of activation (Araque et al. 1999; Chun et al. 2020; Lee et al. 2010; Volterra and Meldolesi 2005; Woo et al. 2012). The SOCE system is highly involved in astrocyte functions, making TFP a valuable pharmacological tool for studying Ca^{2+}- and SOCE-related mechanisms (Lia et al. 2023; Ronco et al. 2014; Toth et al. 2019; Verkhratsky and Parpura 2014). We previously demonstrated that activating astrocytes with OptoSTIM1, an optogenetic tool that induces CRAC-dependent Ca^{2+} influx via light stimulation, alleviates post-stroke disability by increasing astrocytic activity and BDNF expression, mimicking exercise-based rehabilitation (Cho et al. 2025). Notably, TFP induces extracellular Ca^{2+} influx and sustains elevated cytosolic Ca^{2+} levels, an effect not replicated by other drugs (Prakriya and Lewis 2015). From this perspective, TFP represents an attractive pharmacological tool for studying Ca^{2+}-related astrocytic functions. In addition, the SOCE system has attracted significant interest and has been extensively studied; yet, the mechanism of CDI remains controversial. One proposed CDI mechanism is Ca^{2+}/CaM-dependent, and TFP inhibits the dissociation of the STIM1–Orai complex by blocking Ca^{2+}/CaM. Thus, TFP may be a useful pharmacological tool for investigating SOCE regulation.

Beyond astrocytes, cytosolic Ca^{2+}-overload activates apoptotic factors in tumor cells, making Ca^{2+}-overload a therapeutic target in cancer research (Bong and Monteith 2018; Danese et al. 2021). TFP has been utilized to induce apoptosis in various cancers, including breast, colorectal, and lung cancer (Feng et al. 2018; Xia et al. 2019; Yeh et al. 2012). We previously reported that TFP induces glioblastoma cell death and suppresses tumor growth by elevating cytosolic Ca^{2+} levels in tumor cells (Kang et al. 2017). In this study, we identified the STIM1–Orai complex as a key molecular mechanism underlying TFP-induced Ca^{2+} elevation, which exhibits sustained kinetics and likely serves as an apoptosis inducer by mimicking cytosolic Ca^{2+} overload. Interestingly, our data reveal a biphasic dose-dependent effect of TFP on Ca^{2+} signals. At lower concentrations, TFP-induced Ca^{2+} elevation increases proportionally with concentration. However, at higher concentrations (above 50 μM), Ca^{2+} signals decrease in both the rising and plateau phases. During Ca^{2+} imaging under 50 μM TFP treatment, we observed cell shrinkage and vesicle formation, indicating cytotoxicity. These findings suggest that modulating TFP concentration can control the degree of cytosolic Ca^{2+} overload. This makes TFP a valuable tool for studying cellular mechanisms underlying injury and apoptosis, as it can effectively mimic conditions of Ca^{2+}-mediated cell death (Giorgi et al. 2018; Harr and Distelhorst 2010; Orrenius et al. 2003). In summary, TFP's unique properties to induce a sustained Ca^{2+} signal make TFP a valuable pharmacological tool for studying the role of long-lasting Ca^{2+} signals in astrocytes and glioblastoma cells and provide a potential therapeutic tool to induce neuroprotection or apoptosis depending on the concentration.

Author Contributions

J.L. and C.J.L. designed the research. J.L. and W.Y. performed experiments and analysis of data. J.L. drafted the manuscript and prepared the figures. C.J.L. supervised the study. All authors reviewed and edited the manuscript.

Acknowledgments

This study was supported by the Center for Cognition and Sociality (IBS-R001-D2) to C.J.L. from the Institute for Basic Science (IBS), South Korea.

Ethics Statement

All animal care and handling were approved by the Institutional Animal Care and Use Committee of the Institute for Basic Science (IBS-2025-013; Daejeon, Korea).

Conflicts of Interest

The authors declare no conflicts of interest.

Data Availability Statement

The published article includes all datasets generated or analyzed during this study. Data are available upon request.

References

Araque, A., V. Parpura, R. P. Sanzgiri, and P. G. Haydon. 1999. "Tripartite Synapses: Glia, the Unacknowledged Partner." *Trends in Neurosciences* 22, no. 5: 208–215.

Bong, A. H., and G. R. Monteith. 2018. "Calcium Signaling and the Therapeutic Targeting of Cancer Cells." *Biochimica et Biophysica Acta* 1865, no. 11: 1786–1794.

Cahoy, J. D., B. Emery, A. Kaushal, et al. 2008. "A Transcriptome Database for Astrocytes, Neurons, and Oligodendrocytes: A New Resource for Understanding Brain Development and Function." *Journal of Neuroscience* 28, no. 1: 264–278.

Cho, J., S. Lee, Y. H. Kook, et al. 2025. "Optogenetic Calcium Modulation in Astrocytes Enhances Post-Stroke Recovery in Chronic Capsular Infarct." *Science Advances* 11, no. 5: eadn7577.

Chun, H., H. Im, Y. J. Kang, et al. 2020. "Severe Reactive Astrocytes Precipitate Pathological Hallmarks of Alzheimer's Disease via H_2O_2-Production." *Nature Neuroscience* 23, no. 12: 1555–1566.

Clapham, D. E. 2007. "Calcium Signaling." *Cell* 131, no. 6: 1047–1058.

Danese, A., S. Leo, A. Rimessi, et al. 2021. "Cell Death as a Result of Calcium Signaling Modulation: A Cancer-Centric Prospective." *Biochimica et Biophysica Acta* 1868, no. 8: 119061.

Feng, Z., Y. Xia, T. Gao, et al. 2018. "The Antipsychotic Agent Trifluoperazine Hydrochloride Suppresses Triple-Negative Breast Cancer Tumor Growth and Brain Metastasis by Inducing G0/G1 Arrest and Apoptosis." *Cell Death & Disease* 9, no. 10: 1006.

Feske, S., Y. Gwack, M. Prakriya, et al. 2006. "A Mutation in Orai1 Causes Immune Deficiency by Abrogating CRAC Channel Function." *Nature* 441, no. 7090: 179–185.

Fierro, L., and A. Parekh. 1999. "Fast Calcium-Dependent Inactivation of Calcium Release-Activated Calcium Current (CRAC) in RBL-1 Cells." *Journal of Membrane Biology* 168: 9–17.

Garavilla, L. D., L. de Garavilla, N. Vergnolle, et al. 2001. "Agonists of Proteinase-Activated Receptor 1 Induce Plasma Extravasation by a

Neurogenic Mechanism." *British Journal of Pharmacology* 133, no. 7: 975–987.

Giorgi, C., A. Danese, S. Missiroli, S. Patergnani, and P. Pinton. 2018. "Calcium Dynamics as a Machine for Decoding Signals." *Trends in Cell Biology* 28, no. 4: 258–273.

Han, K.-S., G. Mannaioni, C. E. Hamill, et al. 2011. "Activation of Protease Activated Receptor 1 Increases the Excitability of the Dentate Granule Neurons of Hippocampus." *Molecular Brain* 4: 1–12.

Harr, M. W., and C. W. Distelhorst. 2010. "Apoptosis and Autophagy: Decoding Calcium Signals That Mediate Life or Death." *Cold Spring Harbor Perspectives in Biology* 2, no. 10: a005579.

Hoth, M., and R. Penner. 1993. "Calcium Release-Activated Calcium Current in Rat Mast Cells." *Journal of Physiology* 465, no. 1: 359–386.

Hou, X., L. Pedi, M. M. Diver, and S. B. Long. 2012. "Crystal Structure of the Calcium Release-Activated Calcium Channel Orai." *Science* 338, no. 6112: 1308–1313.

Kang, S., J. Hong, J. M. Lee, et al. 2017. "Trifluoperazine, a Well-Known Antipsychotic, Inhibits Glioblastoma Invasion by Binding to Calmodulin and Disinhibiting Calcium Release Channel IP3R." *Molecular Cancer Therapeutics* 16, no. 1: 217–227.

Kang, S. S., K. S. Han, B. M. Ku, et al. 2010. "Caffeine-Mediated Inhibition of Calcium Release Channel Inositol 1, 4, 5-Trisphosphate Receptor Subtype 3 Blocks Glioblastoma Invasion and Extends Survival." *Cancer Research* 70, no. 3: 1173–1183.

Kuboniwa, H., N. Tjandra, S. Grzesiek, H. Ren, C. B. Klee, and A. Bax. 1995. "Solution Structure of Calcium-Free Calmodulin." *Nature Structural Biology* 2, no. 9: 768–776.

Kwon, J., H. An, M. Sa, J. Won, J. I. Shin, and C. J. Lee. 2017. "Orai1 and Orai3 in Combination With Stim1 Mediate the Majority of Store-Operated Calcium Entry in Astrocytes." *Experimental Neurobiology* 26, no. 1: 42–54.

Lee, C. J., G. Mannaioni, H. Yuan, D. H. Woo, M. B. Gingrich, and S. F. Traynelis. 2007. "Astrocytic Control of Synaptic NMDA Receptors." *Journal of Physiology* 581, no. 3: 1057–1081.

Lee, S., B. E. Yoon, K. Berglund, et al. 2010. "Channel-Mediated Tonic GABA Release From Glia." *Science* 330, no. 6005: 790–796.

Li, X., G. Wu, Y. Yang, et al. 2017. "Calmodulin Dissociates the STIM1–Orai1 Complex and STIM1 Oligomers." *Nature Communications* 8, no. 1: 1–14.

Lia, A., G. Sansevero, A. Chiavegato, et al. 2023. "Rescue of Astrocyte Activity by the Calcium Sensor STIM1 Restores Long-Term Synaptic Plasticity in Female Mice Modelling Alzheimer's Disease." *Nature Communications* 14, no. 1: 1590.

Liou, J., M. L. Kim, W. do Heo, et al. 2005. "STIM Is a Ca^{2+} Sensor Essential for Ca^{2+}-Store-Depletion-Triggered Ca^{2+} Influx." *Current Biology* 15, no. 13: 1235–1241.

Maléth, J., S. Choi, S. Muallem, and M. Ahuja. 2014. "Translocation Between PI (4, 5) P2-Poor and PI (4, 5) P2-Rich Microdomains During Store Depletion Determines STIM1 Conformation and Orai1 Gating." *Nature Communications* 5, no. 1: 5843.

Meador, W. E., A. R. Means, and F. A. Quiocho. 1992. "Target Enzyme Recognition by Calmodulin: 2.4 Å Structure of a Calmodulin-Peptide Complex." *Science* 257, no. 5074: 1251–1255.

Orrenius, S., B. Zhivotovsky, and P. Nicotera. 2003. "Regulation of Cell Death: The Calcium–Apoptosis Link." *Nature Reviews Molecular Cell Biology* 4, no. 7: 552–565.

Osawa, M., S. Kuwamoto, Y. Izumi, et al. 1999. "Evidence for Calmodulin Inter-Domain Compaction in Solution Induced by W-7 Binding." *FEBS Letters* 442, no. 2–3: 173–177.

Osawa, M., M. B. Swindells, J. Tanikawa, et al. 1998. "Solution Structure of Calmodulin-W-7 Complex: The Basis of Diversity in Molecular Recognition." *Journal of Molecular Biology* 276, no. 1: 165–176.

Prakriya, M., and R. S. Lewis. 2015. "Store-Operated Calcium Channels." *Physiological Reviews* 95: 1383–1436.

Putney, J. W., Jr. 1986. "A Model for Receptor-Regulated Calcium Entry." *Cell Calcium* 7, no. 1: 1–12.

Rizzuto, R., and T. Pozzan. 2006. "Microdomains of Intracellular Ca^{2+}: Molecular Determinants and Functional Consequences." *Physiological Reviews* 86, no. 1: 369–408.

Ronco, V., A. A. Grolla, T. N. Glasnov, et al. 2014. "Differential Deregulation of Astrocytic Calcium Signalling by Amyloid-β, TNFα, IL-1β and LPS." *Cell Calcium* 55, no. 4: 219–229.

Roos, J., P. J. DiGregorio, A. V. Yeromin, et al. 2005. "STIM1, an Essential and Conserved Component of Store-Operated Ca^{2+} Channel Function." *Journal of Cell Biology* 169, no. 3: 435–445.

Sasakura, D., W. Nunomura, and Y. Takakuwa. 2012. "Dynamic Secondary Structural Changes in Ca^{2+}-Saturated Calmodulin Upon Interaction With the Antagonist, W-7." *Biochemical and Biophysical Research Communications* 423, no. 2: 360–365.

Schmitz, E. A., H. Takahashi, and E. Karakas. 2022. "Structural Basis for Activation and Gating of IP3 Receptors." *Nature Communications* 13, no. 1: 1408.

Taylor, C., and A. Laude. 2002. "IP3 Receptors and Their Regulation by Calmodulin and Cytosolic Ca^{2+}." *Cell Calcium* 32, no. 5–6: 321–334.

Toth, A. B., K. Hori, M. M. Novakovic, N. G. Bernstein, L. Lambot, and M. Prakriya. 2019. "CRAC Channels Regulate Astrocyte Ca^{2+} Signaling and Gliotransmitter Release to Modulate Hippocampal GABAergic Transmission." *Science Signaling* 12, no. 582: eaaw5450.

Vandonselaar, M., R. A. Hickie, W. Quail, and L. T. J. Delbaere. 1994. "Trifluoperazine-Induced Conformational Change in Ca^{2+}-Calmodulin." *Nature Structural Biology* 1, no. 11: 795–801.

Verkhratsky, A., and V. Parpura. 2014. "Store-Operated Calcium Entry in Neuroglia." *Neuroscience Bulletin* 30: 125–133.

Vig, M., C. Peinelt, A. Beck, et al. 2006. "CRACM1 Is a Plasma Membrane Protein Essential for Store-Operated Ca^{2+} Entry." *Science* 312, no. 5777: 1220–1223.

Volterra, A., and J. Meldolesi. 2005. "Astrocytes, From Brain Glue to Communication Elements: The Revolution Continues." *Nature Reviews Neuroscience* 6, no. 8: 626–640.

Weiss, B., W. C. Prozialeck, and T. L. Wallace. 1982. "Interaction of Drugs With Calmodulin: Biochemical, Pharmacological and Clinical Implications." *Biochemical Pharmacology* 31, no. 13: 2217–2226.

Wilson, M. A., and A. T. Brunger. 2000. "The 1.0 Å Crystal Structure of Ca^{2+}-Bound Calmodulin: An Analysis of Disorder and Implications for Functionally Relevant Plasticity." *Journal of Molecular Biology* 301, no. 5: 1237–1256.

Woo, D. H., K. S. Han, J. W. Shim, et al. 2012. "TREK-1 and Best1 Channels Mediate Fast and Slow Glutamate Release in Astrocytes Upon GPCR Activation." *Cell* 151, no. 1: 25–40.

Xia, Y., C. Jia, Q. Xue, et al. 2019. "Antipsychotic Drug Trifluoperazine Suppresses Colorectal Cancer by Inducing G0/G1 Arrest and Apoptosis." *Frontiers in Pharmacology* 10: 1029.

Yang, X., H. Jin, X. Cai, S. Li, and Y. Shen. 2012. "Structural and Mechanistic Insights Into the Activation of Stromal Interaction Molecule 1 (STIM1)." *Proceedings of the National Academy of Sciences* 109, no. 15: 5657–5662.

Yeh, C.-T., A. T. H. Wu, P. M. H. Chang, et al. 2012. "Trifluoperazine, an Antipsychotic Agent, Inhibits Cancer Stem Cell Growth and Overcomes

Drug Resistance of Lung Cancer." *American Journal of Respiratory and Critical Care Medicine* 186, no. 11: 1180–1188.

Zhang, S. L., A. V. Yeromin, X. H. F. Zhang, et al. 2006. "Genome-Wide RNAi Screen of Ca^{2+} Influx Identifies Genes That Regulate Ca2+ Release-Activated Ca^{2+} Channel Activity." *Proceedings of the National Academy of Sciences* 103, no. 24: 9357–9362.

Zhang, Y., K. Chen, S. A. Sloan, et al. 2014. "An RNA-Sequencing Transcriptome and Splicing Database of Glia, Neurons, and Vascular Cells of the Cerebral Cortex." *Journal of Neuroscience* 34, no. 36: 11929–11947.

Zweifach, A., and R. S. Lewis. 1995. "Rapid Inactivation of Depletion-Activated Calcium Current (ICRAC) due to Local Calcium Feedback." *Journal of General Physiology* 105, no. 2: 209–226.